UC Berkeley
UC Berkeley Previously Published Works

Title
Magnetic anisotropy in permalloy antidot square lattice

Permalink
https://escholarship.org/uc/item/8tv188fm

Authors
Wang, TY
Han, H-S
Su, C
et al.

Publication Date
2022-02-01

DOI
10.1016/j.jmmm.2021.168680

Peer reviewed

Magnetic anisotropy in permalloy antidot square lattice

T. Y. Wang[1,2], H.-S. Han[3,4], C. Su[1,2,5], Q. Li[1,6], M. Yang[1,7], Xixiang Zhang[8], Weilun Chao[3], C. Hwang[9], A. Zettl[1,2,5], M. Y. Im[3], and Z. Q. Qiu[1,2,†]

[1]*Department of Physics, University of California at Berkeley, Berkeley, CA, 94720, USA*

[2]*Materials Sciences Division, Lawrence Berkeley National Laboratory, Berkeley, CA, 94720, USA*

[3]*Center for X-ray Optics, Lawrence Berkeley National Laboratory, Berkeley, CA, 94720, USA*

[4]*School of Materials Science and Engineering, Ulsan National Institute of Science and Technology (UNIST), Ulsan, 44919, Republic of Korea*

[5]*Kavli Energy NanoSciences Institute at the University of California, Berkeley, CA, USA*

[6]*National Synchrotron Radiation Laboratory, University of Science and Technology of China, Hefei, Anhui 230029, China*

[7]*Institude of Physical Science and Information Technology, Anhui University, Hefei, Anhui 230601, China*

[8]*Physical Science and Engineering Division (PSE), King Abdullah University of Science and Technology (KAUST), Thuwal 23955-6900, Saudi Arabia*

[9]*Korea Research Institute of Standards and Science, Yuseong, Daejeon 305-340, Korea*

Magnetic anisotropy of Permalloy (Py) antidot square lattice was investigated by torquemetry method using Rotation Magneto-Optic Kerr Effect (ROTMOKE). We find that there exists a field-dependent 4-fold magnetic anisotropy with the easy magnetization axis along the [11] axis of the antidot square lattice. In addition, there also exists an artifact of a uniaxial magnetic anisotropy in ROTMOKE result. We show that both observations are due to the period wiggling of the magnetization in space which was confirmed by magnetic imaging using magnetic transmission soft x-ray microscopy (MTXM). Micromagnetic simulation from MuMax3 supports the wiggling structure of the magnetization, as well as reproduces the artifact of the uniaxial anisotropy. An oversimplified model was developed based on the periodic wiggling of the magnetization and successfully explored the physical origin of the field-dependent 4-fold anisotropy and the artifact of the uniaxial anisotropy.

PACS numbers: 75.70.Ak

1. Introduction

Artificial magnetic nanostructures have attracted much interest due to their novel magnetic properties as well as their application potentials in spintronics technology [1]. While layered magnetic nanostructures usually employ interfacial/interlayer interactions to generate various magnetoelectronic properties such as the giant magnetoresistance [2,3] and tunneling magnetoresistance [4,5], magnetic dots/antidots are generally aimed to modulate spins laterally to create new magnetic states such

as spin ice states [6], and magnetic vortices/skyrmions [7,8,9]. For the latter topic of magnetic dot/antidot nanostructures, array of periodically distributed dots or holes(antidots) are usually created to modulate the magnetization of a thin film at sub-micron length scale using various methods such as lithography, shadow mask growth, and self-assembly, etc [10].

In terms of experimental techniques, magnetic measurement usually involves two types of techniques with one measuring the macroscopic magnetization such as the

torquemetry [11], hysteresis loop comparison [12], and Ferromagnetic Resonance (FMR) [13], etc., with another probing the spatial distribution of the magnetization such as magnetic force microscopy (MFM) [14], photoemission electron microscopy (PEEM) [15], and scanning electron microscopy with spin polarization (SEMPA) [16], etc. Each technique has its strength but also weakness. For example, macroscopic measurement can usually retrieve the anisotropy value from experiment but cannot reveal the microscopic origin. MFM has a high spatial resolution but probes only the stray field produced by the magnetic charges thus usually has to combine with micromagnetic simulation to reconstruct the in-plane magnetization distribution. In contrast, PEEM and SEMPA can probe magnetic component directly in all directions but have to be operated in the absence of external magnetic field. As a practical approach, there is a need to employ several complimentary measurement techniques in order to gain comprehensive information of the magnetic nanostructures.

In terms of magnetic properties in magnetic dot/antidot structures, magnetic anisotropy has been one of the intensely investigated properties because of its important role in high-density magnetic recording [17,18]. The overall goal of this research direction is to achieve a programable magnetic anisotropy [19] by tailoring the geometry of the system such as the shape, size, and spatial distribution of the dot/antidot, etc [20,21,22]. Most of the studies have taken the advantage of magnetic shape anisotropy that magnetic charges at the dot/antidot boundaries introduce additional magnetic dipolar interaction. A representative system is the square lattice of magnetic dots/antidots synthesized from a magnetic thin film. It was found that a 4-fold anisotropy could be induced in such system with the hard magnetization axis along the directions connecting nearest neighboring dots/antidots [13, 23,24,25,26,27]. Although numeric micromagnetic simulations suggest none-uniform spin configurations in the patterned nanostructures [23,28,29,30,31], it has more or less remained obscure on the relation between the magnetic anisotropy and the spin configuration in space. In particular, it is puzzling that the anisotropy magnitude decreases with increasing the applied magnetic field although such dependence offers a new opportunity to tailor the magnetic anisotropy [32]. It is even more mysterious that the torquemetry measurement indicates the existence of a uniaxial anisotropy which

should be absent in a 4-fold symmetric arrays of dots/antidots [23].

In this paper, we report a systematic study of the magnetic anisotropy in permalloy (Py) antidot square arrays. Using rotational magneto-optic Kerr effect (ROTMOKE), we show a clear dependence of the magnetic anisotropy on the magnetic field strength, indicating a spatial variation of the magnetization as the origin of the magnetic anisotropy. By imaging the magnetic structure using full field magnetic transmission soft X-ray microscopy (MTXM), we directly revealed the in-plane wiggling of the Py magnetization and its behavior at different external magnetic fields. This spatial variation of the magnetization also explains the artifact of the uniaxial anisotropy appeared in torquemetry measurement. We further performed micromagnetic simulation and the result agrees nicely of the experimental observations. Finally, we offered a simplified model to reveal the physical origin of the real 4-fold anisotropy and the artifact of uniaxial anisotropy.

2. Experiment

Square lattice of Py antidots was prepared by depositing Py on top of Quantifoil holey carbon grid at room temperature by an e-beam evaporator in an ultrahigh vacuum system with a base pressure of 5×10^{-10} Torr. Py was chosen because it has negligibly small magnetic anisotropy so that magnetic anisotropy in Py antidot square arrays comes entirely from the patterned structure. The holey carbon grid is made of a 15 nm thick holey carbon film containing a square array of 1μm-diameter circular holes with a center-to-center distance of 1.6μm. Py film deposited on top of this holey carbon grid naturally forms a film with arrays of antidot forming at the locations of the holes. The circular shape of the antidot ensures that each dot alone doesn't generate magnetic anisotropy so that the macroscopic anisotropy has to come from the global antidot square lattice. SEM image confirms the formation of the Py antidots with desired sizes (Fig. 1).
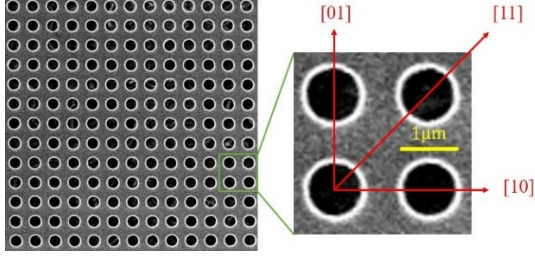
Fig. 1: SEM image of 70 nm-thick Py antidots square array on Quantifoil holey carbon grid.

ROTMOKE measurement was performed at room temperature on the Py antidot sample. The in-plane projection of the incident laser beam was set to be parallel to the nearest neighbor antidots axis. As an in-plane magnetic field rotates in the film plane, the ROTMOKE measures the projection of the magnetization along the optical plane from which the angle between the magnetization and the optical plane could be retrieved. Then the angular difference between the magnetic field and the magnetization contains the information of the magnetic anisotropy. Detailed description of the ROTMOKE instrument and principle can be found in our previous paper [33].

MTXM measurement was performed at room temperature at beamline 6.1.2 of the Advanced Light Source at Lawrence Berkeley National Laboratory. Off-orbit emitted radiation provides elliptically polarized x-rays which illuminates the sample after passing a condenser zone plate. Another micro zone plate then projects a full field image onto a CCD camera that is sensitive to soft x-rays. External magnetic field generated by a solenoid was applied along the x-ray direction so in-plane magnetic field was obtained by tilting the sample at 60° to the x-ray beam, the absorption of x-ray transmitted through the Py film depends on the relative angle between the beam direction and the local magnetization [known as x-ray magnetic circular dichroism (XMCD)], which gives magnetic contrast in the image that directly shows the in-plane magnetization components in the sample [34].

3. Result and Discussion

3.1 MOKE and ROTMOKE result

We first present result of hysteresis loop measured by magnetic-optic Kerr effect (MOKE) and torque curve measured by ROTMOKE on 70 nm thick Py antidot arrays. [10] and [11] directions of the antidot square array are defined in Fig.1. Hysteresis loops for magnetic field along [10] and [11] axes show clearly that it is easier to saturate the magnetization in [11] direction than [10] direction, showing that the magnetic easy axis is parallel to [10] axis.

Next, we present the ROTMOKE result. For an in-plane magnetic field applied to the film with uniform magnetization, the magnetic energy per unit volume is

$$E = -H M_S \cos(\theta - \varphi) - K_2 \cos^2(\varphi - \varphi_2) + K_4 \sin^2(\varphi)\cos^2(\varphi)$$
(1)

where M_S is the saturation magnetization, H is the magnitude of the applied magnetic field, K_2 is the uniaxial magnetic anisotropy, K_4 is the 4-fold magnetic anisotropy, and θ and φ are the angles of the magnetic filed and the magnetization relative to the [10] direction of the antidots lattice, respectively. φ_2 defines the easy ($K_2 > 0$) or hard ($K_2 < 0$) magnetization axis of the uniaxial magnetic anisotropy. Minimizing the energy with respect to φ leads to the magnetic torque [$l(\varphi)$] needed to achieve equilibrium state.

$$l(\varphi) \equiv H \sin(\theta - \varphi) = \frac{1}{2} H_{K_2} \sin[2(\varphi - \varphi_2)¿] + \frac{1}{4} H_{K_4} \sin(4\varphi)¿$$
,
(2)

where $H_{K_2} = 2K_2/M_s$, $H_{K_4} = 2K_4/M_s$ are the uniaxial anisotropy and 4-fold magnetic anisotropy fields, respectively.
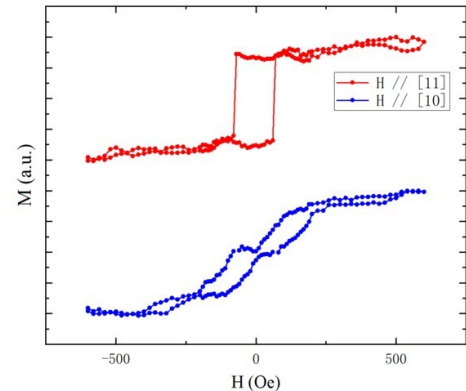

3

Fig. 2: Hysteresis loop along [10] and [11] directions of the Py antidot square lattice measured by MOKE. Hysteresis loop fully closes at around 500 Oe.

To have a unique magnetic torque at a given magnetic field, the field has to be strong enough to wipe out all irreversible magnetic domains. Therefore, we performed ROTMOKE measurement with the magnetic field greater than ~500 Oe above which the hysteresis disappears even along the hard axis (Fig. 2). For a given direction of the field (θ), the magnetization angle (φ) is determined from the ROTMOKE signal which is proportional to $\cos\varphi$. Then the magnetic torque of $H\sin(\theta-\varphi)$ is constructed as a function of φ. Fig. 3 depicts a representative ROTMOKE result at H=600 Oe.

The magnetic torque oscillates with φ with a periodicity of 90° [Fig. 3(a)], showing the existence of a 4-fold magnetic anisotropy. Looking in details, the 4-fold oscillation of the torque doesn't have the same peak height. In fact, the 1st and 3rd peaks have the same height which is less than the height of the 2nd and 4th peaks. This behavior indicates the existence a uniaxial anisotropy ($H_{K_2} \neq 0$) in addition to the 4-fold anisotropy (H_{K_4}). A fitting of the experimental data using eqn. (2) yields $H_{K_2}=-104\pm4$ Oe, $\varphi_2=-2.2\pm1.3°$, and $H_{K_4}=-181\pm10\,Oe$. The negative value of H_{K_4} indicates that [10] and [01] axes are the hard magnetization axes and [11] and [1$\acute{1}$] axes are the easy magnetization axes of the 4-fold magnetic anisotropy.
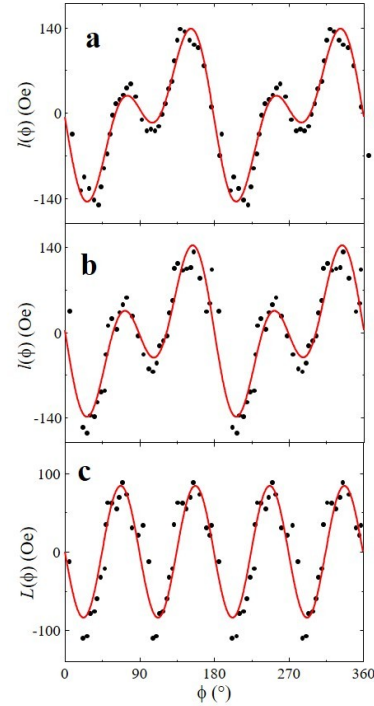

Fig. 3: ROTMOKE result. Magnetic torque $l(\varphi)$ at H = 600 Oe with the optical plane parallel to **a**, [10] axis, and **b**, [01] axis of the sample, respectively. In experiment, (a) and (b) were achieved by fixing the optical plane in space but rotating sample by 90° around the surface normal direction. The identical result of **a** and **b** shows that the uniaxial anisotropy is an artifact. **c**, Redefined torque $L(\varphi)$ using eqn. (3) to eliminate the artifact of the uniaxial anisotropy. Red lines are fitting curves using eqn. (2).

In a system with a perfect 4-fold symmetry, uniaxial magnetic anisotropy is forbidden. However, uniaxial anisotropy could be induced by breaking the 4-fold symmetry such as by different lengths of the antidot along [10] and [01] axes [32] or by off-normal growth of the Py film [35]. Indeed uniaxial anisotropy was shown in torquemetry measurement in square arrays of antidots before without a clear explanation [23]. We checked our sample carefully and find no evidence of elliptical shape of the antidots (Fig. 1). We also grew the Py carefully with normal directional growth by facing the evaporator directly

to the substrate. Therefore, we believe that the uniaxial anisotropy should be an artifact appeared in the torque measurement. To prove this artifact, we rotated the sample by 90º and performed the ROTMOKE measurement again. If the uniaxial anisotropy were real, the easy magnetization axis of the uniaxial anisotropy should be changed by 90º (e.g., φ_2 should increase by 90º) while keeping the 4-fold anisotropy unchanged. Consequently, the magnitudes of the four peaks in Fig. 3(a) would have been changed accordingly with the height of the 1st and 3rd peaks greater than the height of the 2nd and 4th peaks. Our ROTMOKE result after the sample rotation [Fig. 3(b)], however, is identical to the ROTMOKE result before the sample rotation [Fig. 3(a)]. In fact, the same fitting applied to Fig. 3(a) fits Fig. 3(b) perfectly (red color solid line), proving that the uniaxial anisotropy is an artifact in the torque measurement rather than a real existence in the sample. We will discuss the origin of this artifact later in the paper.

To eliminate the artifact of the uniaxial anisotropy in the torque, we reinforce the 4-fold symmetry by redefining the torque as:

$$L(\varphi) = \frac{1}{2}\left[l(\varphi) + l(\varphi + 90^0)\right], 0^0 \leq \varphi \leq 180^0 (3).$$

$L(\varphi)$ obtained in this way [Fig. 3(c)] eliminates the artifact of the uniaxial anisotropy and can be fitted using eqn. (2) with $H_{K_2} = 0$ to obtain the 4-fold anisotropy H_{K_4}. In fact, the H_{K_4} obtained in this way has the same value as the fitting result of H_{K_4} obtained from Fig. 3(a) within the error bar from the fittings.
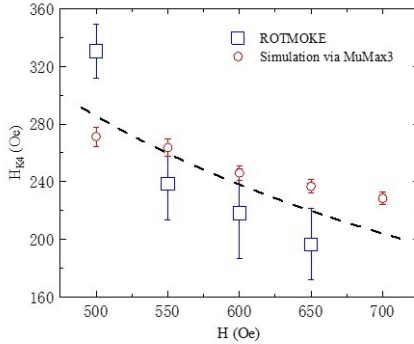

Fig. 4: H_{K4} from ROTMOKE experiment and MuMax3 simulation above 500 Oe. Dashed line represents

$H_{K4} \propto 1/H$ relation from the over-simplified model.

Fig. 4 shows the fitting result of H_{K_4} (blue squares) above 500 Oe (below 500 Oe irreversible hysteresis appears so that ROTMOKE method is no longer valid). The result shows that magnitude of the 4-fold anisotropy decreases with increasing the field, in agreement with result reported in literature [23]. Moreover, we find that the magnitude of the 4-fold anisotropy decreases monotonically with increasing the magnetic field. This behavior implies that the 4-fold magnetic anisotropy should vanish in the limit of $H \rightarrow \infty$. Note that magnetization becomes uniform ($\nabla \vec{M}$ =0) in the limit of $H \rightarrow \infty$ and that the magnetic charge distribution at the boundary of a circular disk with a uniform magnetization corresponds to a magnetic moment at the center of each antidot, the vanish of the 4-fold magnetic anisotropy is nothing but the expected fact that magnetic dipolar interaction does give a 4-fold shape anisotropy for a uniform magnetization in a square lattice (we will give a rigorous proof of this assertion later in this paper). Therefore the none zero 4-fold magnetic anisotropy in our antidot square lattice must come from a none-uniform magnetization in space at finite magnetic field.

3.2 Magnetic images

To prove the none-uniformity of the magnetization in space, we obtained magnetic images of 100 nm thick Py antidot square lattice using MTXM at room temperature. The MTXM images (Fig. 5) with an in-plane magnetic field show clearly that the magnetization is not aligned uniformly to the field direction. Instead, the magnetization tends to move away from the field direction especially at low magnetic field. In particular, the magnetization in region between two nearest-neighbor antidots tends to be parallel to the antidot boundary, resulting a periodic wiggling of the magnetization around the antidot square lattice. The wiggling amplitude of the magnetic texture reduces gradually with increasing magnetic field, approaching a uniform saturation magnetization to the field direction as the in-plane field increases to 1 kOe which is

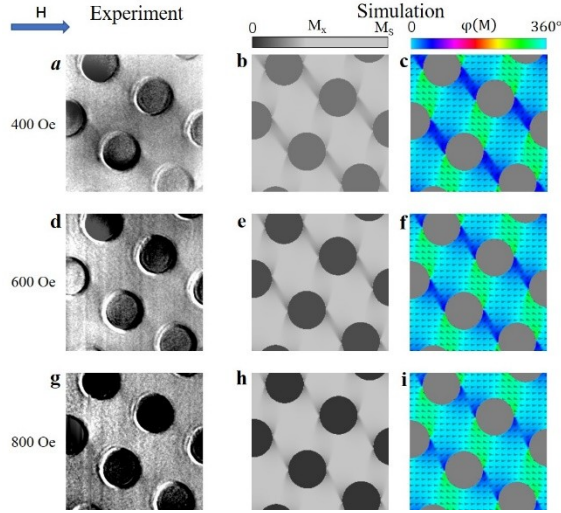the maximum in-plane field available at the MTXM beamline.

Fig. 5: Experimental images from MTXM and simulated images from MuMax3. **a**, **d**, **g:** Experimental MTXM images with in-plane magnetic field of 400, 600 and 800 Oe, respectively, along the direction as shown on the top left. **b**, **e**, **h:** Simulated MTXM images with the x-component of magnetization (M_x) represented by the greyscale colormap shown on top. **c**, **f**, **i:** Colored images showing the magnetization direction in space. The colormap on top shows the magnetization angle $\varphi(M)$ relative to the field direction.

Qualitatively, the wiggling of the magnetization can be understood by considering the magnetic charges at the antidot boundary. For a uniform magnetization along the field direction, magnetic charges are induced at the antidot boundary. To reduce the magnetic dipolar interaction energy, magnetic charges at the antidot boundary should be reduced by rotating the magnetization between two nearest-neighbor antidots along [10] axis towards the [01] or [0$\bar{1}$] direction. Similarly, the magnetization between two nearest-neighbor dotes along [01] axis should rotate towards [10] or [$\bar{1}$0] direction to reduce the magnetic charges at the antidot boundary. Therefore, a uniform magnetization in the field direction should rotate in

opposite directions along the [10] and [01] axes to reduce the magnetic charges at the antidot boundaries, leading to a periodic wiggling of the magnetization in the antidot square lattice. Since this wiggling of magnetization is at the expanse of Zeeman energy by rotating the magnetization away from the magnetic field direction, the wiggling amplitude should be obviously reduced by increasing the magnetic field.

3.3 Micromagnetic simulation

To have a quantitative analysis, we have to consider a continuous variation of the magnetization in whole space. To do so, we performed micromagnetic simulation using MuMax3 on a 100nm Py thick antidot film with the same geometry parameters as in the experiment. The simulation result (Fig. 5) indeed shows the same trend of wiggling magnetization as observed by the MTXM with the wiggling amplitude decreasing with increasing magnetic field. Furthermore, we find that the wiggling magnetization follows exactly 4-fold symmetry as the magnetic field direction rotates. This is expected because in simulation we could ensure a prefect 4-fold symmetry of the antidot system.

Then the interesting question is if an artifact of uniaxial anisotropy would appear in the ROTMOKE torque measurement from a simulation on a perfect 4-fold antidot square lattice? To answer this question, we performed micromagnetic simulation of the process of ROTMOKE via MuMax3 on a 10×10 Py antidot square lattice (70 nm Py thickness, $1\mu m$-diameter hole, and $1.6\mu m$ period) for a rotating in-plane magnetic field of H=500 ~ 700 Oe. For each step of the magnetic field angle (θ), equilibrium state of the magnetization in the MuMax3 simulation was achieved by relaxing the equilibrium state of the magnetization of the previous step. Because of the perfect 4-fold symmetry of our system, it turns out that simulation was needed only for $0^0 \leq \theta \leq 90^0$ and simulation result for $90^0 \leq \theta \leq 360^0$ can be simply obtained by extending the result of $0^0 \leq \theta \leq 90^0$ to the corresponding angular range. In this way, we obtained the magnetic state in the whole range of field angle from 0^0 to 360^0 with 5^0 per step. Next, for each field angle θ, we calculated the averaged projection of the magnetization to the [10] axis (

$M_x = \frac{1}{N}\sum_{i=1}^{N} cos\varphi_i$) which is what ROTMOKE measures directly in experiment. The maximum value of M_x among all field angles is set to be the saturation magnetization (M_s) and then the averaged magnetization angle $\varphi \equiv \arccos\left(\frac{M_x}{M_s}\right)$ and magnetic torque $l(\varphi) = H sin(\theta - \varphi)$ were obtained from the simulation and compared to the experimental ROTMOKE result. One of the simulated torque curves is shown in Fig. 6.
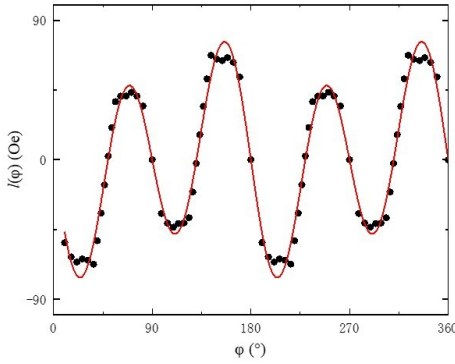

Fig. 6: An example of simulated torque $l(\varphi)$ via MuMax3 at H = 600 Oe.

The $l(\varphi) vs \varphi$ relation obtained from the simulation agrees nicely with the ROTMOKE experiment result. H_{K_4} values obtained by fitting the simulated $l(\varphi) vs \varphi$ at several field strengths are shown in Fig. 4 for comparison with the experimental result. We would like to point out a few essential features from the simulation. First, it is clear that the magnetic anisotropy arises from the none-uniformity of the magnetization in space, i.e., it is the wiggling of the magnetization in space that makes the spatially averaged φ different from the θ. Specifically, it is the magnetization between nearest neighbor antidots, which prefers its orientation parallel to [10] or [01] axis, that results in the macroscopic magnetic anisotropy. Second, the different peak heights in $l(\varphi)$ (e.g., the 1st and 3rd peak heights are less than the 2nd and 4th peak heights) show that an artifact of uniaxial anisotropy appears in the simulated $l(\varphi) vs \varphi$ relation, in agreement with the experimental observation [Fig. 3(a) and (b)]. As shown in the next section, it is the

broadening of the angular distribution of the magnetization that leads to the artifact of the uniaxial anisotropy.

3.4 Simplified model

While the micromagnetic simulation successfully reproduces experimental result, physical origin of the result also becomes obscured somewhat in the numerical calculations. To explore the physical origin, we here discuss an oversimplified model to explain the 4-fold magnetic anisotropy and the artifact of uniaxial anisotropy in terms of the magnetization wiggling in space. We start by considering a two-dimensional antidot square lattice in xy plane with an in-plane magnetization. The total dipolar energy of the system is

$$E_d = \sum \frac{\vec{m}(\vec{r})\cdot\vec{m}(\vec{r}\,') - 3\,\vec{m}(\vec{r})\cdot(\widehat{\vec{r}-\vec{r}\,'})\,\vec{m}(\vec{r}\,')\cdot(\widehat{\vec{r}-\vec{r}\,'})}{|\vec{r}-\vec{r}\,'|^3}$$

(4)

Using $\varphi(\vec{r})$ to specify the local angle between the local magnetic moment and the [10] axis of the antidot square lattice, it is easy to show that the change of dipolar energy due to magnetization wiggling of $\varphi(\vec{r}) = \varphi_M + \delta\varphi(\vec{r})$ to the leading order of $\delta\varphi(\vec{r})$ is

$$\delta E_d = 3\sin(2\varphi_M)\sum \frac{[\delta\varphi(\vec{r})+\delta\varphi(\vec{r}\,')][(x-x')^2-(y-y')^2]}{2|\vec{r}-\vec{r}\,'|^5}$$

.   (5)

We have employed the result of $\sum \frac{\delta\varphi(\vec{r})(x-x')(y-y')}{|\vec{r}-\vec{r}\,'|^5} = \sum \frac{\delta\varphi(\vec{r}\,')(x-x')(y-y')}{|\vec{r}-\vec{r}\,'|^5} = 0$ in the derivation because of the inversion symmetry and the 4-fold symmetry of the antidot square lattice with circular shaped antidot.

For uniform magnetization, $\delta\varphi(\vec{r})$ is independent of position so that $\varphi(\vec{r}) = \varphi_M + const.$ corresponds to a uniform rotation of a uniform magnetization. Then eqn. (5) yields $\delta E_d = 0$ because a 4-fold symmetry yields $\sum \frac{(x-x')^2-(y-y')^2}{2|\vec{r}-\vec{r}\,'|^5} = 0$. This is the result mentioned

in previous sections that dipolar interaction from a uniform magnetization in a square antidot lattice with 4-fold symmetry doesn't give raise any magnetic anisotropy.

To have a none-zero δE_d, the local magnetic moments at $\vec{r}$ and $\vec{r}'$ need to twist oppositely [e.g., $\delta\varphi(\vec{r})$) and $\delta\varphi(\vec{r}')$ have opposite signs] as $(x-x')^2-(y-y')^2$ changes its sign under the action of $x \leftrightarrow y$. This corresponds to the scenario that the magnetization between neighboring antidots along [10] axis rotates in opposite direction as the magnetization between neighboring antidots along [01] axis. In another word, the magnetization needs to wiggle oppositely along the [01] and [01] axes in order to give raise a none-zero magnetic anisotropy of $\delta E_d \neq 0$, which is exactly what was observed in our experiment. The physical origin of the opposite twisting angles of the magnetization along [1] and [01] axes is that the neighboring antidots along [10] axis prefer the magnetization along [01] axis, which is equivalent to a local uniaxial anisotropy with [01] axis being the magnetization easy axis. Similarly, neighboring antidots along [01] axis leads to an equivalent local uniaxial anisotropy with [10] axis being the magnetization easy axis. To make this physical picture clearer, we further simplified the model by breaking the magnetization texture into two subsystems of $\vec{M}_1$ and $\vec{M}_2$ with $\vec{M}_1$ and $\vec{M}_2$ experiencing local uniaxial anisotropies (K) of [10] and [01] easy magnetization axis, respectively (Fig. 7). Although not accurate, this oversimplified model can catch the physical origin of all experimental observations.
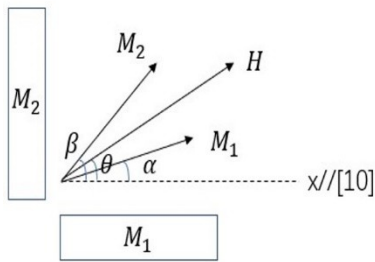

Fig. 7: In our oversimplified model, M_1 and M_2 are the magnetizations of the two domains whose magnetic easy axes are parallel to [10] and [01] axes, respectively. As a magnetic field H is applied at an angle θ to the [10] axis, M_1 and M_2 will tilt away

from their own easy axes, resulting angles of α and β to the [10] axis. In this case, $\alpha < \theta < \beta$.

Without the two local uniaxial magnetic anisotropies or in the limit of $H \rightarrow \infty$, it is obvious that a uniform magnetization of $\vec{M}_1 = \vec{M}_2$ should be aligned to the magnetization field direction ($\vec{H}$), leading to an absence of the magnetic anisotropy. Adding the weak two local uniaxial anisotropies, $\vec{M}_1$ should rotates slightly away from the field direction towards its [10] easy axis ($\varphi_1 < \theta$) and $\vec{M}_2$ should rotates slightly away from the field direction towards its [01] easy axis ($\varphi_2 > \theta$), leading to the opposite twisting angles of $\vec{M}_1$ and $\vec{M}_2$. With the averaged magnetization angle of $\varphi_M \equiv (\varphi_2 + \varphi_1)/2$ and the small twisting angle amplitude of $\delta \equiv (\varphi_2 - \varphi_1)/2$, it is easy to show that the magnetic energy is

$$E = -K\cos^2\varphi_1 - H M_S \cos(\theta - \varphi_1)$$

$$+ K\cos^2\varphi_2 - H M_S \cos(\theta - \varphi_2)$$

$$\dot{\iota} 2\cos\delta[-K\sin(2\varphi_M)\sin\delta - H M_S \cos(\theta - \varphi_M)] (6)$$

Minimizing the energy with respect to small δ and φ_M, we obtained the following result.

$$\delta = \frac{K}{H M_S}\sin(2\varphi_M) \quad (7)$$

$$H \sin(\theta - \varphi_M) = \frac{-K^2}{H M_S^2}\sin(4\varphi_M) \quad (8)$$

Eqn. (8) corresponds to the torque eqn. (2) with a 4-fold anisotropy only ($H_{K_4} = \frac{-12 K^2}{H M_S}$). Therefore our oversimplified model not only reproduces correctly the 4-fold anisotropy with [11] easy magnetization axis ($H_{K_4} < 0$) but also a monotonically decrease of the anisotropy with increasing the magnetic field. In fact, the $H_{K_4} \propto 1/H$ relation in eqn. (8) describes the experimental result fairly well (dashed line in Fig. 4). The [11] easy magnetization axis can be understood easily from this oversimplified model that for magnetic field applied in the [11] direction (

$\vec{H}$//[11]), it is obvious that $\vec{M}_1$ and $\vec{M}_2$ should deviate away from $\vec{H}$ direction symmetrically towards [10] and [01], respectively, leading to an averaged magnetization $(\vec{M}_1+\vec{M}_2)/2$ exactly in the $\vec{H}$ direction (e.g. easy magnetization axis).

Last, we would like to discuss the artifact of a uniaxial magnetic anisotropy in ROTMOKE measurement. Precisely speaking, ROTMOKE measures the averaged projection of the magnetization to the [10] axis ($\cos\acute{\varphi}=\frac{1}{N}\sum_{i=1}^{N}cos\varphi_i$) and then converts the result to the averaged magnetization angle by $\acute{\varphi}=\arccos\left(\frac{1}{N}\sum_{i=1}^{N}cos\varphi_i\right)$. For uniform magnetization, this process makes no difference between $\acute{\varphi}$ and the magnetization angle of φ_M. Fore none-uniform magnetization, however, the magnetization angle determined by ROTMOKE is slightly greater than the averaged magnetization angle ($\acute{\varphi}>\varphi_M=\frac{1}{N}\sum_{i=1}^{N}\varphi_i$). It is this difference between $\acute{\varphi}$ and φ_M that results in the artifact of a uniaxial anisotropy in ROTMOKE simply because $Hsin(\theta-\acute{\varphi})\neq Hsin(\theta-\varphi_M)$. To understand this artifact more clearly, we again use the oversimplified model to discuss how the difference between $\acute{\varphi}$ and φ_M results in a uniaxial anisotropy term in eqn. (8). Using the relation of $\cos\acute{\varphi}=¿$ and eqn. (7), it is easy to derive the difference between $\acute{\varphi}$ and φ_M for small δ.

$$\varphi_M=\acute{\varphi}-\left(\frac{K}{HM_S}\right)^2\sin(2\acute{\varphi})\cos^2(\acute{\varphi}) \quad (9)$$

Substitute eqn. (9) into eqn. (8) leads to

$$Hsin(\theta-\acute{\varphi})=\frac{-K^2}{2HM_S^2}\sin(2\acute{\varphi})-\frac{5K^2}{4HM_S^2}\sin(4\acute{\varphi})$$
(10)

The first term at the right side of eqn. (10) corresponds to the uniaxial anisotropy in eqn (2) with $H_{K_2}<0$ and $\varphi_0=0$, in agreement with experimental observation. While eqn. (10) describes the experimental result qualitatively well, we would like to emphasize that the oversimplified model ignores many factors such as the coupling between $\vec{M}_1$ and $\vec{M}_2$ and the spatial variation within $\vec{M}_1$ and $\vec{M}_2$. All these factors are expected to modify the strength of H_{K_2} and H_{K_4} in eqn. (2) from the model. Nevertheless, the oversimplified model correctly reveals the physical origin of the field-dependent 4-fold anisotropy and the artifact of the uniaxial anisotropy.

3. Summary

In summary, we investigated the magnetic anisotropy of Py antidot square lattice using ROTMOKE. We showed that there exists a field-dependent magnetic anisotropy which is originated from the periodic wiggling of the magnetization in space. This none or un-uniformity of the magnetic texture was confirmed by magnetic imaging using MTXM as a function of magnetic field. We also clarified the puzzle of the unexpected uniaxial magnetic anisotropy as an artifact due to the magnetization wiggling in space. Micromagnetic simulation result agrees very well with the experimental observation. We further proposed an oversimplified model to qualitatively explain the physical origin of the field-dependent 4-fold anisotropy and the artifact of the uniaxial anisotropy. Our investigation provides direct observation and explanation of the magnetic anisotropies in antidot square lattice.

References:

[1] .S. S. P. Parkin and S. D. Bader, *Annual Review of Condensed Matter Physics* **1**, 71 (2010).

[2] .G. Binasch, P. Grunberg, F. Saurenbach, and W. Zinn, *Phys. Rev. B* **39**, 4828 (1989).

[3] .M. N. Baibich, J. M. Broto, A. Fert, F. Nguyen Van Dau, F. Petroff, P. Etienne, G. Creuzet, A. Friederich, and J. Chazelas, *Phys. Rev. Lett.* **61**, 2472 (1988).

[4] .T. Miyazaki & N. Tezuka, *J. Magn. Magn. Mater.* **139**, L231 (1995).

[5] .J. S. Moodera, Lisa R. Kinder, Terrilyn M. Wong, and R. Meservey, *Phys. Rev. Lett*. **74**, 3273 (1995).

[6] .Sandra H. Skjærvø, Christopher H. Marrows, Robert L. Stamps, and Laura J. Heyderman, *Nature Reviews Physics* **2**, 13 (2020).

[7] .T. Shinjo1, T. Okuno, R. Hassdorf, K. Shigeto, T. Ono, *Science* **289**, 930 (2000).

[8] .J. Li, A. Tan, K. W. Moon, A. Doran, M. A. Marcus, A. T. Young, E. Arenholz, S. Ma, R. F. Yang, C. Hwang and Z. Q. Qiu, *Nat. Commun.* **5**, 4704 (2014).

[9] .S. Saha, M. Zelent, S. Finizio, M. Mruczkiewicz, S. Tacchi, A. K. Suszka, S. Wintz, N. S. Bingham, J. Raabe, M. Krawczyk, and L. J. Heyderman, *Phys. Rev*. *B* **100**, 144435 (2019).

[10] .J. IMartĺn, J. Nogués, Kai. Liu, J. L. Vicent, and Ivan K Schuller, *J. Magn. Magn. Mater.* **256**, 449 (2003).

[11] .A. Lisfi, C. M. Williams, L. T. Nguyen, J. C. Lodder, A. Coleman, H. Corcoran, A. Johnson, P. Chang, A. Kumar, and W. Morgan, *Phys. Rev. B* **76**, 054405 (2007).

[12] .L. G. Vivas, M. Vazquez, J. Escrig, S. Allende, D. Altbir, D. C. Leitao, and J. P. Araujo, *Phys. Rev. B* **85**, 035439 (2012)

[13] .Sam D. Slöetjes, Einar Digernes, Christoph Klewe, Padraic Shafer, Q. Li, M. Yang, Z. Q. Qiu, Alpha T. N'Diaye, Elke Arenholz, Erik Folven, and Jostein K. Grepstad, *Phys. Rev. B* **99**, 064418 (2019).

[14] .U. Hartmann, *Annual Review of Materials Science* **29**, 53 (1999).

[15] .X M Cheng and D J Keavney, *Rep. Prog. Phys.* **75**, 026501 (2012).

[16] .S. Y. Chou, *Proceedings of the IEEE* **85**, 652 (1997).

[17] .M Salaheldeen, L Martínez-Goyeneche, P Álvarez-Alonso, and A. Fernández, *Nanotechnology* **31** 485708 (2020).

[18] .Shanshan Guo, Feng Xu, Baomin Wang, Ning Wang, Huali Yang, Pravarthana Dhanapal, Fei Xue, Junling Wang, Run-Wei Li, *Adv. Mater. Interfaces* **5**, 1800997, (2018).

[19] .Jiyun Kim, Su Eun Chung, Sung-Eun Choi, Howon Lee, Junhoi Kim, and Sunghoon Kwon, *Nat. Mater.* **10**, 747 (2011).

[20] .A. O. Adeyeye and N Singh, *J. Phys. D: Appl. Phys.* **41** 153001 (2008).

21 .S. Finizio, M. Foerster, M. Buzzi, B. Krüger, M. Jourdan, C. A. F. Vaz, J. Hockel, T. Miyawaki, A. Tkach, S. Valencia, F. Kronast, G. P. Carman, F. Nolting, and M. Kläui, *Phys. Rev. Applied* **1**, 021001 (2014).

22 .Na Zhu, Houchen Chang, Andrew Franson, Tao Liu, Xufeng Zhang, E. Johnston-Halperin, Mingzhong Wu, and Hong X. Tang, *Appl. Phys. Lett.* **110**, 252401 (2017).

23 .C. T. Yu, H. Jiang, L. Shen, P. J. Flanders, and G. J. Mankey, J. Appl. Phys. 87, 6322–6324 (2000).

24 .P. Vavassori, *J. of Appl. Phys.* **91**, 7992 (2002).

25 .G. N. Kakazei, X. M. Liu, J. Ding, V. O. Golub, O. Y. Salyuk, R. V. Verba, S. A. Bunyaev, and A. O. Adeyeye, *Appl. Phys. Lett.* **107**, 232402 (2015).

26 .Andreas Kaidatzis, Rafael P del Real, Raquel Alvaro, Juan Luis Palma, José Anguita, Dimitrios Niarchos, Manuel Vázquez, Juan Escrig, and José Miguel García-Martín, *Appl. Phys. Lett.* **107**, 232402 (2015).

27 .G. N. Kakazei, X. M. Liu, J. Ding, V. O. Golub, O. Y. Salyuk, R. V. Verba, S. A. Bunyaev, and A. O. Adeyeye, *J. Phys. D: Appl. Phys.* **49**, 175004 (2016).

28 .C. C. Wang, A. O. Adeyeye, and N. Singh, *Nanotechnology* **49**, 1629 (2006).

29 .O. N. Martyanov, V. F. Yudanov, R. N. Lee, S. A. Nepijko, H. J. Elmers, R. Hertel, C. M. Schneider, and G. Schönhense, *Phys. Rev. B* **75**, 174429 (2007).

30 .Agne Ciuciulkaite, Erik Östman, Rimantas Brucas, Ankit Kumar, Marc A. Verschuuren, Peter Svedlindh, Björgvin Hjörvarsson, and Vassilios Kapaklis, *Phys. Rev. B* **75**, 174429 (2007).

31 .O. N. Martyanov, V. F. Yudanov, R. N. Lee, S. A. Nepijko, H. J. Elmers, R. Hertel, C. M. Schneider, and G. Schönhense, *Phys. Rev. B* **99**, 184415 (2019).

32 .Xiaolong Fan, Hengan Zhou, Jinwei Rao, Xiaobing Zhao, Jing Zhao, Fengzhen Zhang and Desheng Xue, *Scientific Reports* **5**, 16349 (2015).

33 .J. Li, E. Jin, H. Son, A. Tan, W. N. Cao, Chanyong Hwang, and Z. Q. Qiu, *Review of Scientific Instruments* **83**, 033906 (2012).

34 .Peter Fischer, Dong-Hyun Kim, Weilun Chao, J. Alexander Liddle, Erik H. Anderson, and David T. Attwood, *Materials Today* **9**, 26 (2006).

35 .J. H. Wolfe, R. K. Kawakami, W. L. Ling, and Z. Q. Qiu, Rodrigo Arias, and D. L. Mills, *J. of Magn. Magn. Mat.* **232**, 36 (2001).